Fabrication of TiO_2/CdS heterostructure photoanodes and optimization of light scattering to improve the photovoltaic performance of dye sensitized solar cells (DSSCs)

S. Revathi
Muthayammal College of Arts and Science
A Pricilla Jeyakumari (pricilla1510@gmail.com)
Thiruvalluvar Government Arts College https://orcid.org/0000-0003-4134-2085

Research Article

Keywords: TiO2, CdS, Heterojunction, Microwave, Photo-conversion efficiency, Dye sensitized solar cell

Posted Date: February 18th, 2021

DOI: https://doi.org/10.21203/rs.3.rs-187929/v1

Version of Record: A version of this preprint was published at Journal of Materials Science: Materials in Electronics on April 10th, 2021. See the published version at https://doi.org/10.1007/s10854-021-05822-9.

Abstract

Currently, the TiO2/CdS photoanodes based dye sensitized solar cells (DSSCs) have shown extraordinary developments in the photo conversion efficiency. In this report, pristine TiO2, CdS and various molar ratios of TiO2/CdS photoanodes were prepared by one step microwave irradiation route and followed by doctor blade method. The sheet like morphology of the TiO2 and CdS nanoparticles were clearly evident from the SEM and TEM images. A significant reduction band gap with enhanced light absorption and rapid prevention of electron hole pair was explored by UV-DRS and PL studies. The photocurrent density-voltage (J-V) and electrochemical impedance (EIS) characteristics were analyzed for assembled solar cell. The photo-conversion efficiency of 12.8% was obtained with the configuration TiO2/CdS (200 mg) that represent a 2.5 fold increment compared to bare TiO2 (5.33%) as well as commercial Pt (6.11%). The experimental results are discussed.

1. Introduction

Recently, Photovoltaic cell (PV) has poor conversion power efficiency from light to electricity. Behind the overlay of many PV device that produce over than 41% of the incident light output electricity and semiconductor materials have a performance was lower than 20% as a results of the greatest usage of enterprise. Because, these PVs can translate only the quarter part of the light output obtained. This performance can restrict by certain chemical composition of the component [1-3]. Solar energy is also one of the greatest significant power renewable resources due to its continuous supply and economic compatibility [4-7]. Solar cells, which transfer solar energy directly into electrical energy and heat, can decrease energy costs incurred by alternate energy generation. It is well known that titanium oxide (TiO_2) is one of the important photoanodes in the DSSCs due to its outstanding physico-chemical properties, suitable electronic structure and band-gap energy [8-10]. In pristine TiO_2, electron mobility is also too limited and thus lower solar cell transfer efficiency [11, 12]. A large number of works has been done to increase light quality in a visible light area by concentrating on the development of high-performance sensitizers [13–16]. A substrate to absorb photographs in the full sunlight spectrum remains a task. Semiconductor materials like CdSe, CdS, Bi_2S_3, PbS, $CdTe_2$ and $CuInS_4$, and so on that adsorb visible light may act as sensitizers even though they are capable of transmitting electricity to wide semiconductors such as pristine ZnO and TiO_2 [17]. Variety of methods have been used to fabricate the TiO_2/CdS heterostructure such as Hydrothermal. Solvothermal, microwave dielectric, chemical bath deposition, sol gel and chemical co-precipitation methods and so on.

Among these, Microwave irradiation has an absorption function that makes it easy to heat up the solution uniformly. The effect is uniform ionization and rapid crystal growth, leading to the development of limited distribution crystallites [18]. Compared to other traditional approaches, microwave irradiation synthesis has the benefit of a fast response time, which is due to the occupying power produced by microwave electrical or magnetic factors that produce friction and molecular interactions. In the present investigation, the novel TiO_2/CdS binary photoanodes was synthesized by facile microwave irradiation

method for the first time without employing the hydrothermal process. The constructed TiO_2/CdS binary photoanodes exhibits high photo-conversion efficiency and good electro catalytic activity with long term stability performance than bare TiO_2 and CdS. The origin of this high photovoltaic property was investigated through various experimental studies such as powder X-ray diffraction (XRD), TEM, UV-Vis DRS, SEM, XPS and Photovoltaic were studies. The improved photovoltaic mechanism of the proposed DSSC was also discussed in detail.

2. Experimental

2.1 Materials

All the chemicals used were analytical grade used without any further purification. They are Titanium isopropoxide (TTIP, 99% Sigma–Aldrich), cadmium nitrate [$Cd(NO_3)_2$,$4H_2O$] (98% Fisher Scientific) and sodium thiosulfate [$Na_2S_2O_3$, $5H_2O$] (98% Sigma–Aldrich).

2.2 Synthesis of TiO_2, CdS and TiO_2/CdS nanocomposite samples

The synthesis process of photoanodes was convoluted in numerous steps. In order to prepare TiO_2 sample, 10 ml of TTIP was hydrolyzed with mixed solution of water and ethanol (1:1). After that NaOH was added to the TiO_2 in order to increase the PH value of the solution as 9. The resultant product was placed to microwave oven and irradiated at 140 ^oC for 10 min. Finally, the product was dried at conventional mode (100 ^oC for few hours). In the preparation of CdS nanoparticles, 0.5 g of $Cd(NO_3)_2$,$4H_2O$ and 2 g of $Na_2S_2O_3$, $5H_2O$ was separately diluted with 50 ml of deionized water (DI). The mixture was placed to microwave oven and irradiated at 140 ^oC for 10 min. Finally, the product was dried at conventional mode (100 ^oC for few hours). In TiO_2/CdS nanocomposite preparation, the various amounts of CdS (25, 50 and 100 mg) were mixed with TiO_2 with mechanical grinding method. The different ratio of CdS (25, 50 and 100 mg) with TiO_2 was marked as TiO_2/CdS25, TiO_2/CdS50 and TiO_2/CdS100, respectively.

2.3. DSSC fabrication setup

The present solar cell device is sandwich type, which is consists of photoanode, cathode and electrolyte solution, respectively. The photoanode and cathode of DSSC is fabricated using TiO_2/CdS and commercial platinum (Pt) paste deposition on FTO substrate using doctor blade method [19]. Then the photoanode was immersed in N719 dye solution. 0.6 M iodide/triiodide liquid electrolyte was injected between photoanode and cathode, respectively. AM1.5, 100 $mWcm^{-2}$ solar stimulator was used to monitor the photocurrent vs. voltage characteristics. The active surface area of the DSSC was 0.16 cm^2 (0.4 x 0.4 cm^2).

2.4 Characterization techniques

X-ray diffraction (XRD) (Japan, XD-3A) using CuKα radition and a scintillation counter detector were used to identify the crystalline structure of the samples. The morphological and optical properties of the samples were analyzed by Hitachi SU8010 type SEM instrument, H-600-II, Hitachi type TEM analytical instrument, UV–Vis spectrophotometer (UV-2550, Shimadzu, Japan). The electronic structure and chemical composition of the sample were determined by XPS (AXIS-165 Shimadzu, Japan). Autolab Potentiostate ECO CHEMIE was used to monitor the electrochemical performance.

3. Results And Discussion

3.1 Structural characteristics

The crystallinity structure is investigated using the Powder XRD pattern and the pertinent pattern is seen in the Figure 1.The sharp peaks in X-ray diffraction of pristine TiO_2 assay suits well with the TiO_2 anatase phase with tetragonal crystalline structure (JCPDS N. 89-4921) with the following matched miller orientation planes of (101), (004), (200) (105), (211) and (204) respectively. While the wurtzite structure of CdS was confirmed with relative diffraction planes of (002), (110), (103), and (112), consequently. The results matched perfectly with the standard data (JCPDS No.65–3414). The mixture orientation plane of TiO_2 ((101), (200), (211), (204)) and CdS ((002), (110), (103), and (112)) in the composite samples reveal the formation of heterostruture between them. It was renowned that no other additional or impurity phases were found in the pattern, which resembles the high product purity. The anatase and wurtzite structure of TiO_2 and CdS was further confirmed by Raman spectroscopy, which is shown in Figure 2. The Raman modes of 517 cm^{-1} (A_{1g} antisymmetric bending quivering of O-Ti-O), and 638 cm^{-1} (E_g) [20], confirmed the anatase phase of TiO_2. The high intensity bands assigned to CdS at 300 cm^{-1} and 604 cm^{-1} [21]. The increase of cds content in the TiO_2 were significantly enhanced the property, which was identified by the Raman intensity modes. This attributed to the structural distortion between heterostructure crystal matrices.

3.2. Morphological analysis

Figure 3 (a-c) shows the SEM images of pure TiO_2, CdS and TiO_2/CdS100, samples respectively. The sheet like and spherical nanoparticles were identified in the pristine TiO_2 and CdS nanoparticles. In the TiO_2/CdS100 composite, the CdS nanoparticles are anchored on the surface of TiO_2 nanosheets. Further the TEM image of pristine TiO_2 sample clearly expose the wrinkle type ultrathin nanosheets (diameter in several micrometers) were identified (Fig. 3d). The clear individual spherical nanoparticles (30-40 nm) of CdS were also noticed in the corresponding TEM picture (Fig. 3e). The CdS nanoparticles were clearly decorated on the TiO_2 nanosheets surface in the TiO_2/CdS100 composite (Fig. 3f). The elemental mapping of TiO_2/CdS100 composite clearly exhibits the presence of the key elements of Ti, O, Cd and S (Fig. 3 g-j). The results yet again substantiate the formation of heterostructure between TiO_2 and CdS.

3.3. Optical characteristics

UV-Vis DRS was implemented to discern the skill of light absorption and optical band gap energy of the samples. Figure 4a) shows the UV absorption spectra of all the samples. The absorption values of pristine TiO_2 and CdS were located at 410 and 480 nm, respectively. The K-M model [22, 23] has been utilized to extrapolate the band gap energy and the relevant band gap plot is shown in Figure 4b). The calculated band gap energy of TiO_2 and CdS was 3.02 eV and 2.58 eV. The light absorption ability is significantly improved in the visible light region when the loading amount of CdS is increased in to TiO_2. After combination of CdS with TiO_2, the band gap energy was gradually decreased from 3.02 eV to 2.25 eV. This could be due to the heterostructure combination adequate to extended light absorbance ability, which is favorable to enhancing the DSSC power conversion efficiency in the photovoltaic field. The luminescence and charge transfer process of the samples were further analyzed by room temperature photoluminescence spectra with excitation wavelength of 350 nm and the emission spectrum is shown in Figure 5. The abroad emission intensity in the visible light (440 nm) and green light (545 nm) region is perceived in TiO_2 and CdS samples, respectively. The composite sample cover the emission nature in the visible to green emission region. This may be due to the high luminescence properties of heterostructure combination, which is suitable for optoelectronic device applications. Remarkably, the emission intensity peak was decreased gradually while increasing the CdS content. It was noted that TiO_2/CdS100 sample shows highly reduced emission intensity than compared to other samples. This could be due to the suppress recombination process of electron-hole pair.

3.4. Surface area and chemical composition analysis

Figure 6 (a) & (b) shows the N_2 adsorption-desorption with pore size distribution curves of pure TiO_2, CdS and TiO_2/CdS100, samples respectively. The clear H3 hysteresis loop with type IV isotherm could be noticed in all the samples. Hence, all the samples belong to the mesoporous nature [24-27]. The type IV isotherm is due to the highly porous nature of nanosheets with uniform size of the nanoparticles. The Brunauer-Emmett-Teller (BET) surface area and Barrett-Joyner-Halenda (NJH) pore size of TiO_2/CdS100 composite sample is found to be 103.5 m^2/g and 23.5 nm. The pore size and surface area is higher than pristine TiO_2 (66.8 m^2/g and 37.8 nm) and CdS (45.7 m^2/g and 43.5 nm). The high porous nature of the TiO_2/CdS100 composite sample is due to the uniform size nanoparticles of CdS were successfully decorated on the ultrathin TiO_2 nanosheets surface. Chemical environment and surface element analysis was explored through XPS and the TiO_2/CdS100 composite sample XPS spectra is shown in Figure 7. Figure 7 a) shows the survey spectra with wide range analysis, which is mainly exhibits the major elements of Ti, Cd, O and S. The high magnification spectra of Ti 2p exhibits the binding energies of ~465.1eV and 458.1 eV are ascribed to the $Ti2p_{1/2}$ and $Ti2p_{3/2}$, respectively (Fig. 7b). The Cd 3d core level XPS spectrum (Fig. 7c) has two peaks at 404.1eV (Cd $3d_{5/2}$) and 410.1 eV (Cd $3d_{3/2}$). The high resolution S 2p spectra (Fig. 7d) shows two peaks at 161.4 eV and 164.1 eV, which are related to the $S2p_{1/2}$ and S $2p_{3/2}$. The deconvolution of the XPS spectrum for the O 1s peak is presented in Fig. 7e which is composed of three peaks at 529.1 531.51 and 533.5 eV. These peaks can be consigned to the incident of the Ti-O, C-O, bonds and even S-O/S=O bonds (in sulfate sort) present in the composite.

3.5. Photovoltaic studies

The present DSSC device was sandwich type, which is schematically expressed in Figure 8a). The fabricated DSSC was tested for photo current density – voltage (J-V) characteristics under AM 1.5 solar condition with intensity of 100 mwcm^{-2}. Figure 8b) shows the J-V curves, which shows the photovoltaic parameters of photoelectric conversion efficiency (η), open current voltage (V_{oc}), fill factor (FF) and current density (J_{sc}). The results are précised in Table 1. The optimized TiO_2/CdS100 photoanode show high current density (22.45%) and photo-voltage (932 mV), which results in high PCE of 12.8%. the PCE of TiO_2 and CdS was found to be 5.33 and 3.21%, respectively. The fabricated DSSC was also examined to incident photon to electron conversion efficiency (IPCE) and the plot is display in Figure 8c). The highest IPCE values reaches to 93.5% for optimized TiO_2/CdS100 photoanode than compared with other photoanode samples (at wavelength of 480 nm). The improved IPCE of the composite electrode is attributed to the recombination of lower charge, this leads to greater efficiency gathering of charges and cost effective charging at the interface of the TiO_2/CdS/FTO. In the examination of long term stability test (Fig. 8d), the experiment was carried out with various time solar light illuminations (0-600 h). The results reveal that no major changes in PCE arise throughout the period of testing (approximately 600 h). This could be due to the long term cyclibility of the DSSC. Charge transport and recombination resistance behavior was further analyzed by electrochemical impedance spectra (EIS) analysis. Figure 9 a) shows the Nyquist plot with equivalent circuit (inset) of the all the photoanodes with corresponding circuit. There are two semicircles smaller (lower frequency region) and higher (higher frequency region) was found in the Nyquist plot. The second semicircle was taken to find out the recombination resistance and charge transport properties. The EIS results establish that the optimized TiO_2/CdS100 photoanode show lower RCT (24.5 Ω) and Rs (5.8 Ω) than compared with other photoanode samples. Moreover, the photoanode show longer electron life time (12.5 ms). The EIS parameters values are also summarized in Table 2. The improved mechanism of the DSSC is shown schematically in Figure 9c). The integration of CdS as a photoanode into TiO_2 increases the transport of charges and decreases the recombination of charges because of the greater surface area, resulting in a consistent electron pathway and more dye-binding domains. In addition, the heterostructure consumes more light than the straight bare TiO_2 and CdS. Hence it has higher power conversion efficiency. Moreover, the heterostructure could provide more active site, which means less grain borders, which consequently enhances electrical conductivity and furthermore boosts solar cell performance [28].

4. Conclusions

In the present investigation, the incorporated CdS can fascinate the structural, optical and photovoltaic properties of TiO_2 photoanodes. The sheet like morphology of the TiO_2 and CdS nanoparticles were clearly evident from the SEM and TEM images. The photocurrent density-voltage (J-V) and electrochemical impedance (EIS) characteristics were analyzed for assembled solar cell. The photo-conversion efficiency of 12.8% was obtained with the configuration TiO_2/CdS (200 mg) that represent a 2.5 fold increment compared to bare TiO_2 (5.33%) as well as commercial Pt (6.11%). The enhanced PCE

of the TiO_2/CdS composite is due to the photogenerated electrons can move from CdS to TiO_2 more quickly, ensuring that two dimensional constructs, and their near interfacial touch. Moreover, CdS behaves as an supply of electrons for TiO_2. This special arrangement for electron-hole transition allows for photogenic electrons-holes with a certain electrical potential energy in CB and VB, thereby improving photo-conversion efficiency of DSSC.

References

[1] I. Robel, V. Subramanian, M. Kuno, P.V. Kamat, Quantum Dot Solar Cells. Harvesting Light Energy with CdSe Nanocrystals Molecularly Linked to Mesoscopic TiO_2 Films, J. Am. Chem. Soc. 128 (2006) 2385–2393.

[2] R.S. Selinsky, Q. Ding, M.S. Faber, J.C. Wright, S. Jin, Quantum dot nanoscale heterostructures for solar energy conversion, Chem. Soc. Rev. 42 (2013) 2963–2985.

[3] K. Kalyanasundaram, M. Gratzel, Themed issue: nanomaterials for energy conversion and storage, J. Mater. Chem. 22 (2012) 24190–24194.

[4] B. Li, L. Wang, B. Kang, P. Wang, Y. Qiu, Review of recent progress in solid-state dye-sensitized solar cells, Sol. Energy Mater. Sol. Cells 90 (2006) 549–573.

[5] M. Law, L.E. Greene, J.C. Johnson, R. Saykally, P. Yang, Nanowire dye-sensitizedsolar cells, Nat. Mater. 4 (2005) 455–459.

[6] Tina X. Ding, Jacob H. Olshansky, Stephen R. Leone, A. Paul Alivisatos, Efficiency of hole transfer from photoexcited quantum dots to covalently linked molecular species, J. Am. Chem. Soc. 137 (2015) 2021–2029.

[7] I. Ka, B. Gonfa, V. Le Borgne, D. Ma, M.A. El Khakani, Pulsed laser ablation based synthesis of PbS-quantum dot-decorated one-dimensional nanostructures and their direct integration into highly efficient nanohybrid heterojunction-based solar cells, Adv. Funct. Mater. 24 (2014) 4042–4050.

[8] B. O'Regan, M. Gratzel, A low-cost, high-efficiency solar cell based on dye-sensitized colloidal TiO_2 films, Nature 353 (1991) 737–740.

[9] M. Gratzel, Photoelectrochemical cells, Nature 414 (2001) 338–344.

[10] M. Gratzel, Conversion of sunlight to electric power by nanocrystalline dye-sensitized solar cells, Journal of Photochemistry and Photobiology A: Chemistry 164(2004) 3–14.

[11] P.E. De Jongh, D. Vanmaekelbergh, Trap-Limited Electronic Transport in Assemblies of Nanometer-Size TiO2 Particles, Physical Review Letters 77 (1996) 3427–3430.

[12] G. Schlichthorl, S.Y. Huang, J. Sprague, A.J. Frank, Band Edge Movement and Recombination Kinetics in Dye-Sensitized Nanocrystalline TiO2 Solar Cells: A Study by Intensity Modulated Photovoltage Spectroscopy, Journal of Physical Chemistry B 101 (1997) 8141–8155.

[13] T. Bessho, E. Yoneda, J.H. Yum, M. Guglielmi, L. Tavernelli, H. Lmai, U. Roth-lisberger, M.K. Nazeeruddin, M. GrÃ¤tzel, New Paradigm in Molecular Engineering of Sensitizers for Solar Cell Applications, Journal of the American Chemical Society 131 (2009) 5930–5934.

[14] P.G. Bomben, K.C.D. Robson, P.A. Sedach, C.P. Berlinguette, On the viability of cyclometalated Ru (II) complexes for light-harvesting applications, Inorganic Chemistry. 48 (2009) 9631–9643.

[15] P.G. Johansson, J.G. Rowley, A. Taheri, G.J. Meyer, S.P. Singh, A. Islam, L. Han, Long Wavelength Sensitization of TiO_2 by Ru Diimine Compounds with Low-Lying π* Orbitals,Langmuir 27 (2011) 14522–14531.

[16] H.C. Zhao, J.P. Harney, Y.T. Huang, J.H. Yum, M.K. Nazeeruddin, M. Gratzel, M.K. Tsai,Evaluation of a ruthenium oxyquinolate architecture for dye-sensitized solar cells, J. Rochford, Inorganic Chemistry 51 (2012) 1–3.

[17] H. Jia, H. Xu, Y. Hu, Y. Tang, L. Zhang, TiO_2@CdS core–shell nanorods films: fabrication and dramatically enhanced photoelectrochemical properties, Electrochemistry Communications 9 (2007) 354–360.

[18] H. Yin, T. Yamamoto, Y. Wada, S. Yanagida, Large-scale and size-controlled synthesis of silver nanoparticles under microwave irradiation. Mater. Chem. Phys. 83 (2004) 66–70

[19] Hayder Hasan Ali, Majid R. Al-Bahrani, Synthesis of TiO_2/Graphene Quantum Dots as Photoanode to Enhance Power Conversion Efficiency for Dye-Sensitized Solar Cells, International Journal of Advanced Science and Technology, 29(3), 11071 - 11081.

[20] V. Gombac, L. De Rogatis, A. Gasparotto, G. Vicario, T.Montini, D.Barreca, G. Balducci, Fornasiero, E. Tondello, M.Graziani, TiO_2nanopowders doped with boron and nitrogen for photocatalytic applications, Chemical Physics. 339 (2007) 111–123

[21] J. C. Tristão, F. Magalhães, P. Corio, and M. T. C. Sansiviero, Electronic characterization and photocatalytic properties of CdS/TiO_2 semiconductor composite, Journal of Photochemistry and Photobiology A: Chemistry. 181 (2006) 152–157.

[22] M. Parthibavarman, S. Sathishkumar, M. Jayashree, R. BoopathiRaja, Microwave Assisted Synthesis of Pure and Ag Doped SnO_2 Quantum Dots as Novel Platform for High Photocatalytic Activity Performance, Journal of Cluster Science 30 (2019) 351-363

[23] M. Parthibavarman, S. Sathishkumar, S. Prabhakaran, M. Jayashree, R. BoopathiRaja, High visible light-driven photocatalytic activity of large surface area Cu doped SnO_2 nanorods synthesized by novel one-step microwave irradiation method, Journal of the Iranian Chemical Society 15 (2018) 2789-2801

[24] R. BoopathiRaja, M. Parthibavarman, A. Nishara Begum, Hydrothermal induced novel $CuCo_2O_4$ electrode for high performance supercapacitor applications. Vacuum. 165(2019) 96-104

[25] R. BoopathiRaja, M. Parthibavarman, Hetero-structure arrays of $MnCo_2O_4$ nanoflakes@ nanowires grown on Ni foam: Design, fabrication and applications in electrochemical energy storage, Journal of Alloys and Compounds. 811 (2019) 152084

[26] R. BoopathiRaja, M. Parthibavarman, A Nishara Begum Design and fabrication of hierarchical heterostructure $CuCo_2O_4$@PPy based asymmetric device with ultra high capacitance and attractive cycling performance Materials Research Bulletin 126 (2020) 110817

[27] R. BoopathiRaja, M. Parthibavarman Desert rose like heterostructure of $NiCo_2O_4$/NF@ PPy composite has high stability and excellent electrochemical performance for asymmetric super capacitor application Electrochimica Acta 346 (2020) 136270

[28] S. Biswas, M.F. Hossain, T. Takahashi, Fabrication of Grätzel solar cell with TiO_2/CdS bilayered photoelectrode. Thin Solid Films. 517 (2008) 1284– 1288.

Tables

Table.1 J-V characteristics parameters of the photoanodes

Parameters	TiO_2	CdS	Pt	TiO_2/CdS25	TiO_2/CdS50	TiO_2/CdS100
Jsc (mA/cm^2)	12.8	6.45	15.23	16.81	18.51	22.45
Voc (mV)	670	601	721	742	878	932
Fill Factor	65.1	63.4	68.4	74.1	83.1	88.5
Efficiency η (%)	5.33	3.21	6.11	8.22	9.71	12.8

Table.2 Electrochemical parameters of the photoanodes

Samples	Rs/Ωcm^2	Rct/Ωcm^2	r/ns
CdS	9.4	79.4	4.2
TiO_2	8.2	64.2	6.5
TiO_2/CdS25	7.2	48.9	7.8
TiO_2/CdS50	6.4	38.7	9.2
TiO_2/CdS100	5.8	24.5	12.5

Figures

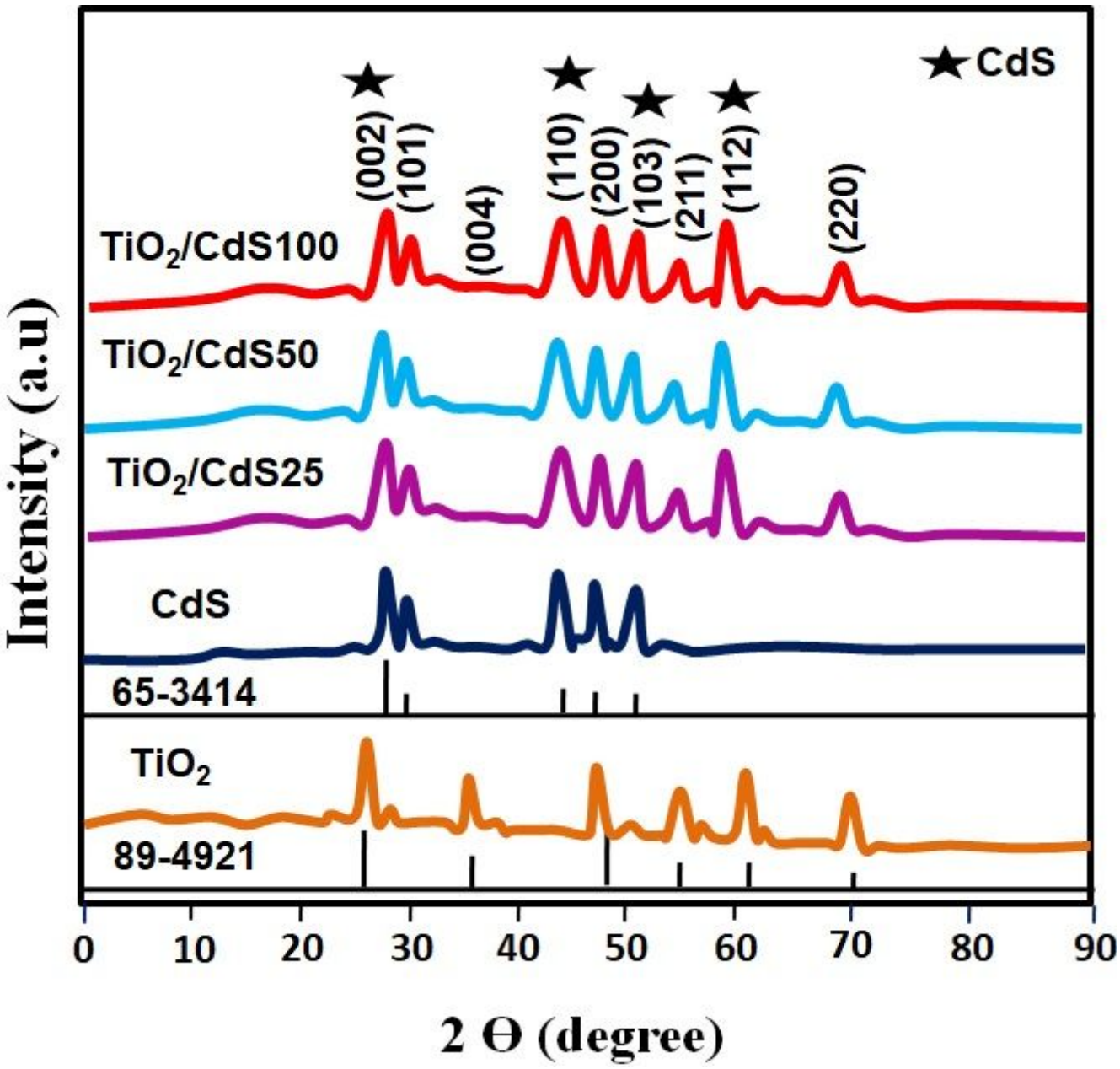

Figure 1

XRD pattern of the photoanodes

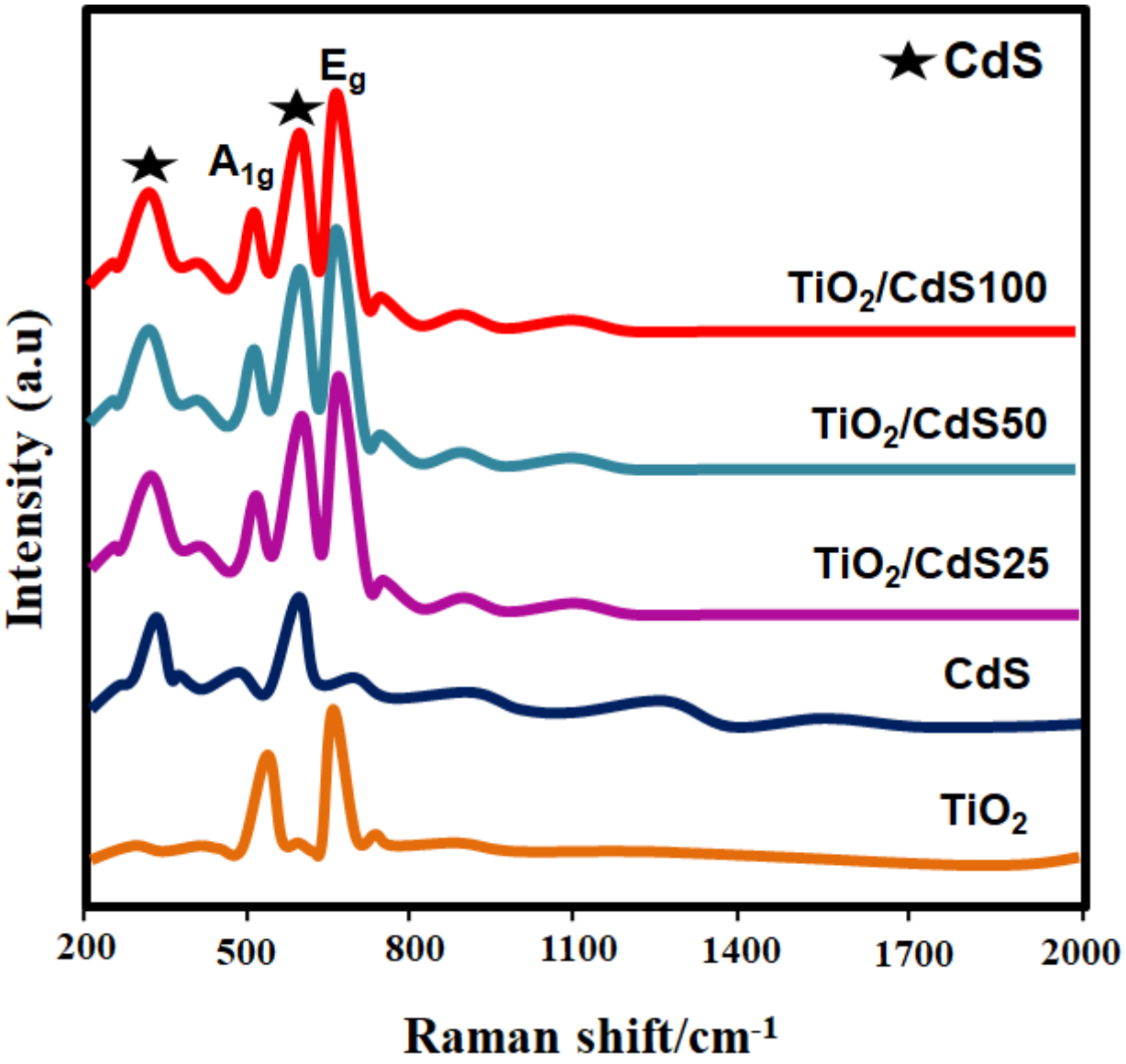

Figure 2

Raman spectra of the photoanodes

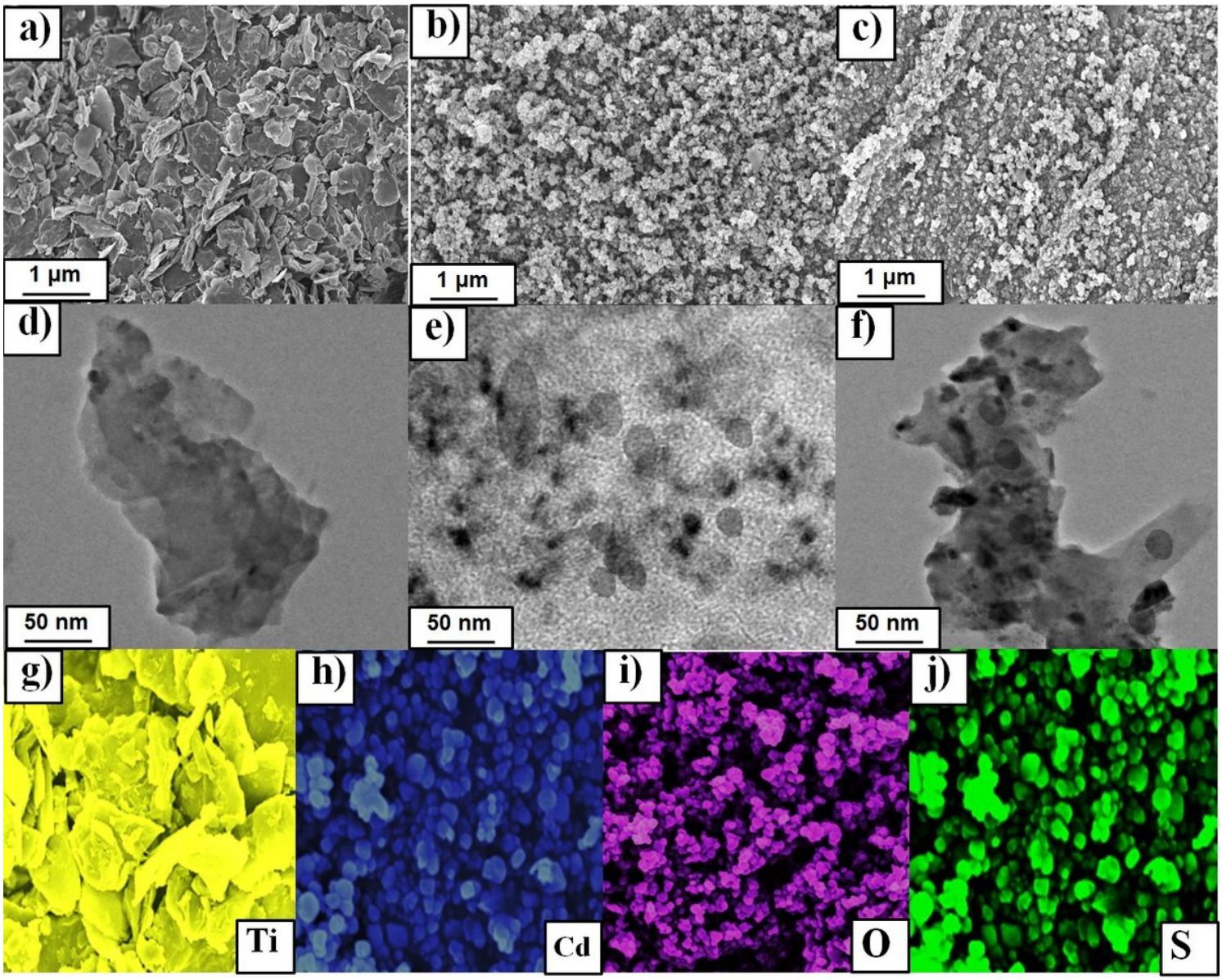

Figure 3

SEM images of a) TiO2; b) CdS; c) TiO2/CdS100; TEM images of d) TiO2; e) CdS; f) TiO2/CdS100; Elemental mapping images of g) Ti; h) Cd; i) O and j) S

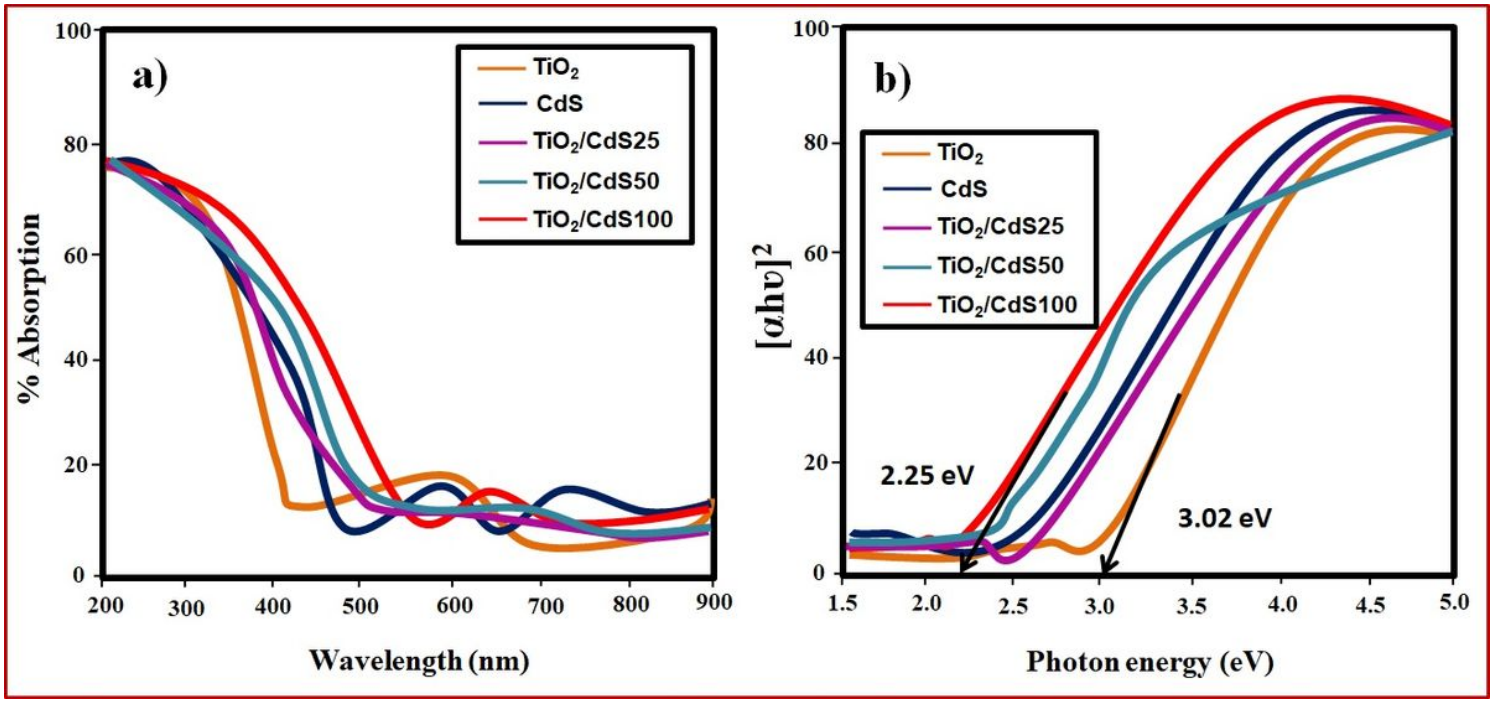

Figure 4

UV-Vis DRS absorption spectra; b) band gap plot

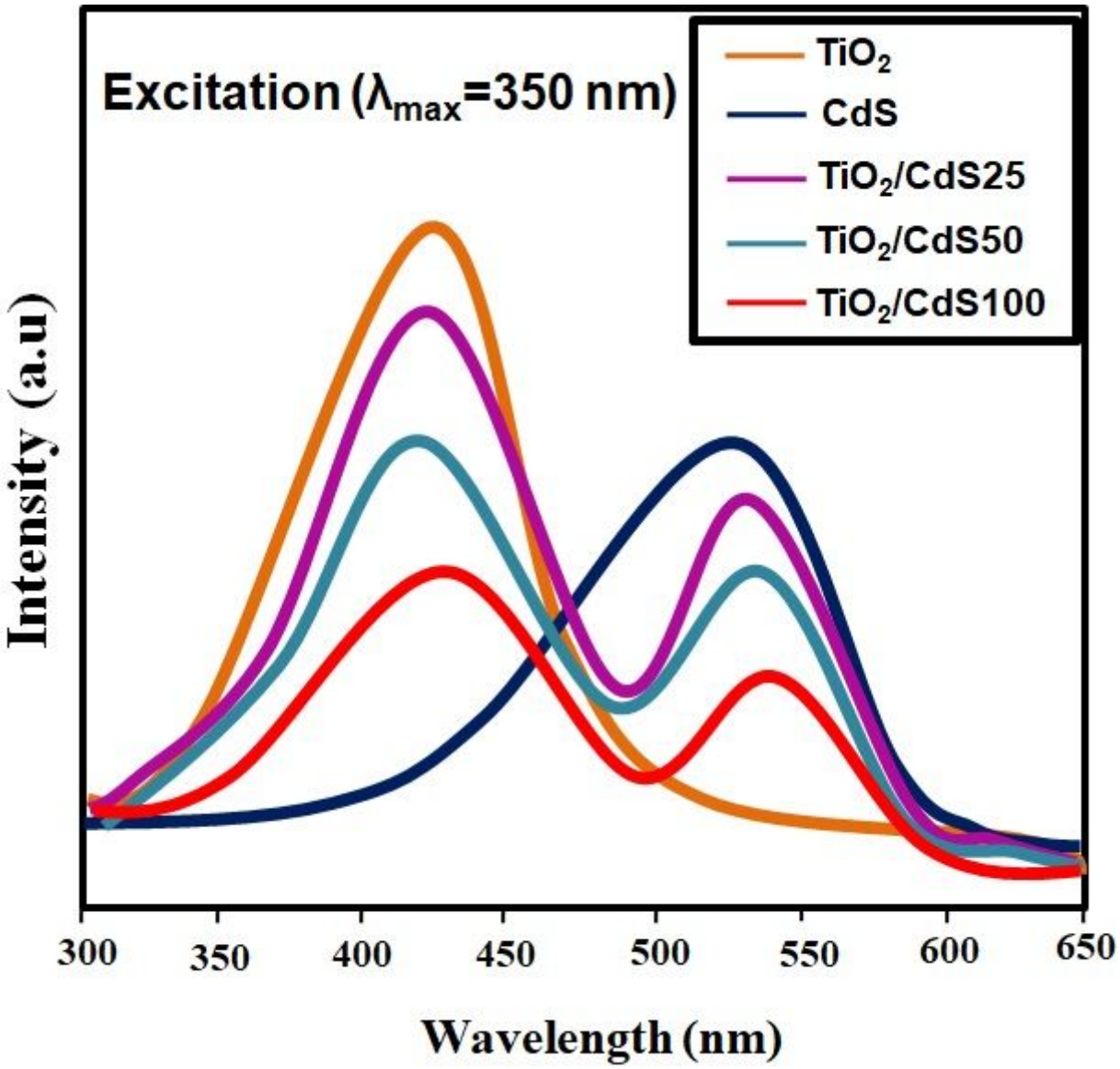

Figure 5

Photoluminescence spectra of the photoanodes

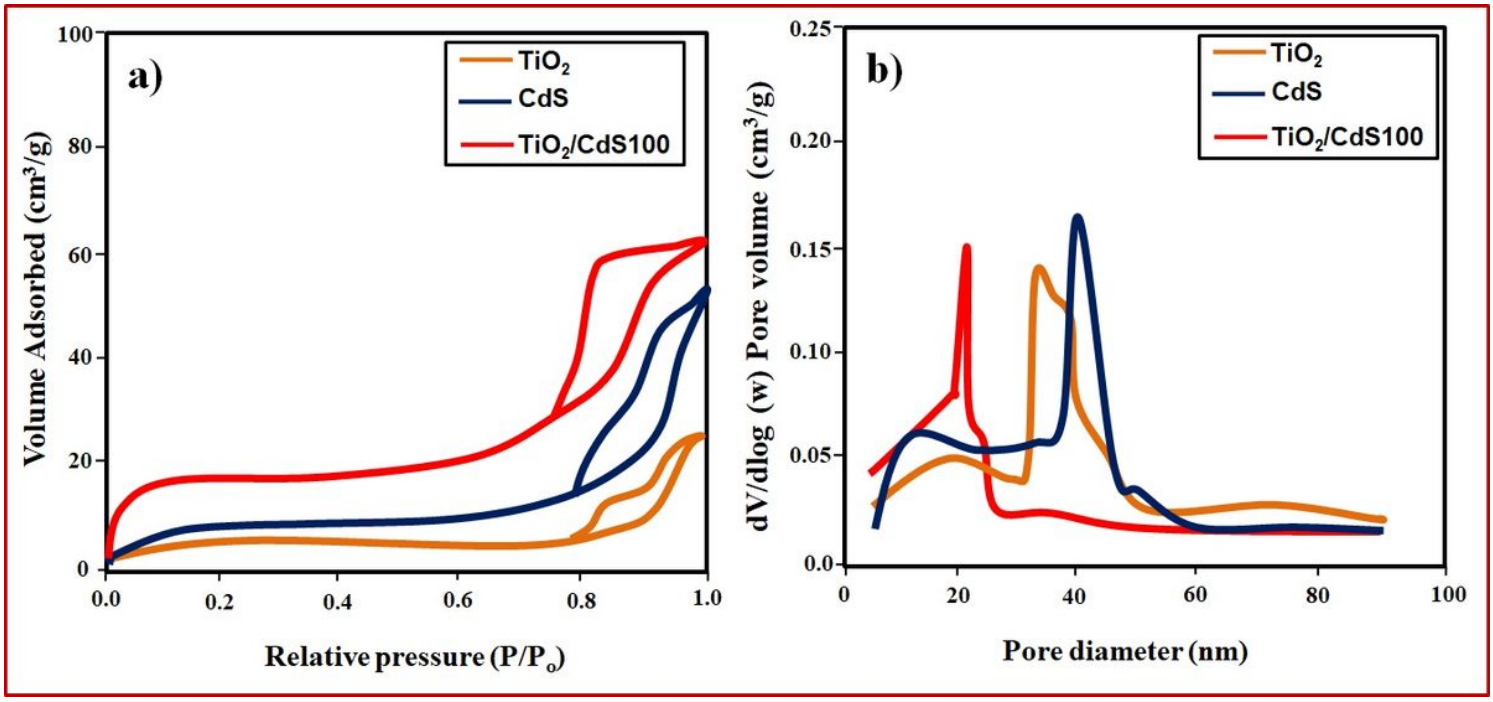

Figure 6

a) N2 adsorption and desorption analysis TiO2, CdS and TiO2/CdS100 samples; b) corresponding pore size distribution

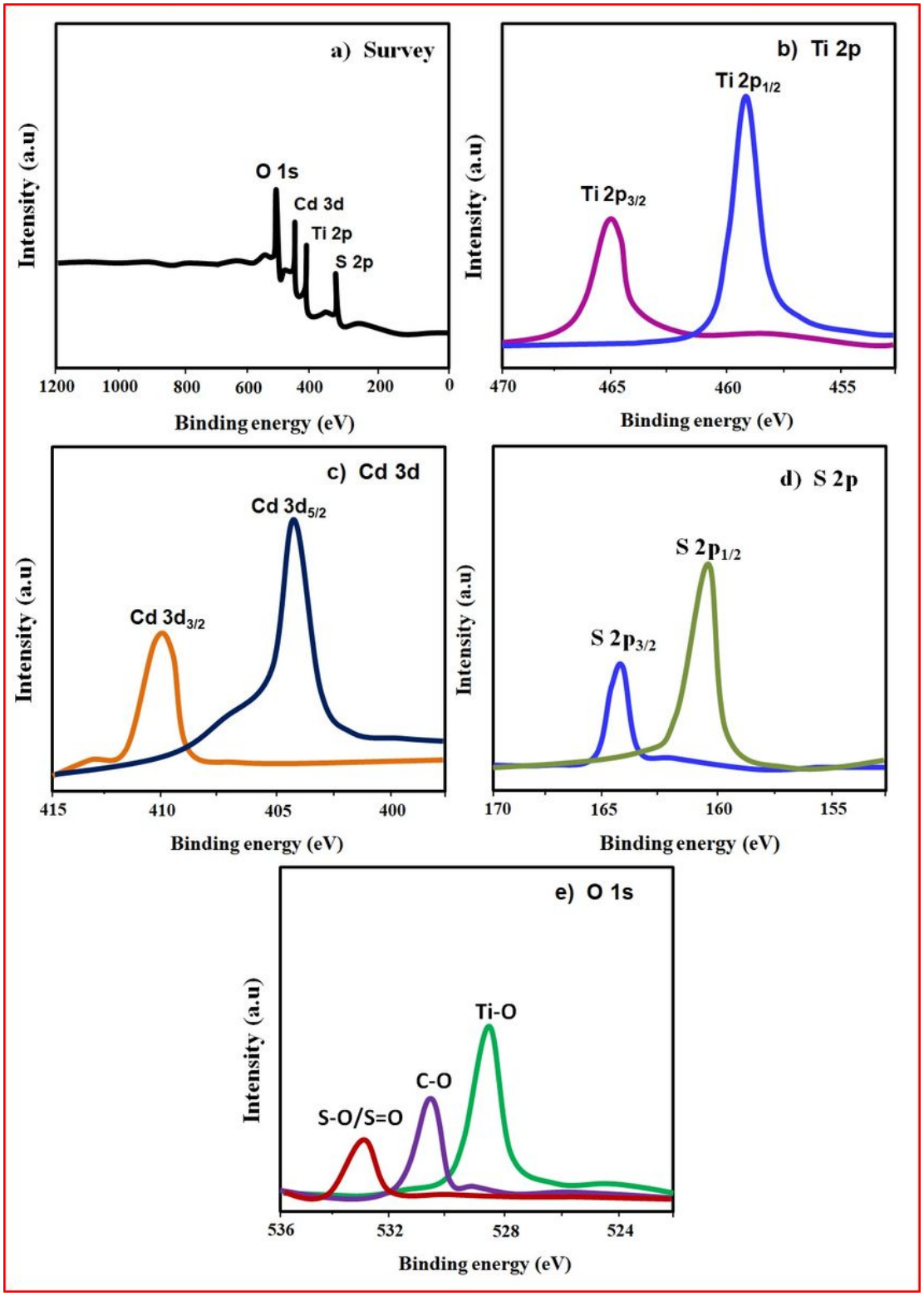

Figure 7

XPS spectra of TiO2/CdS100 sample a) survey; b) Ti 2p; c) Cd 3d; d) O 1s and e) S 2p

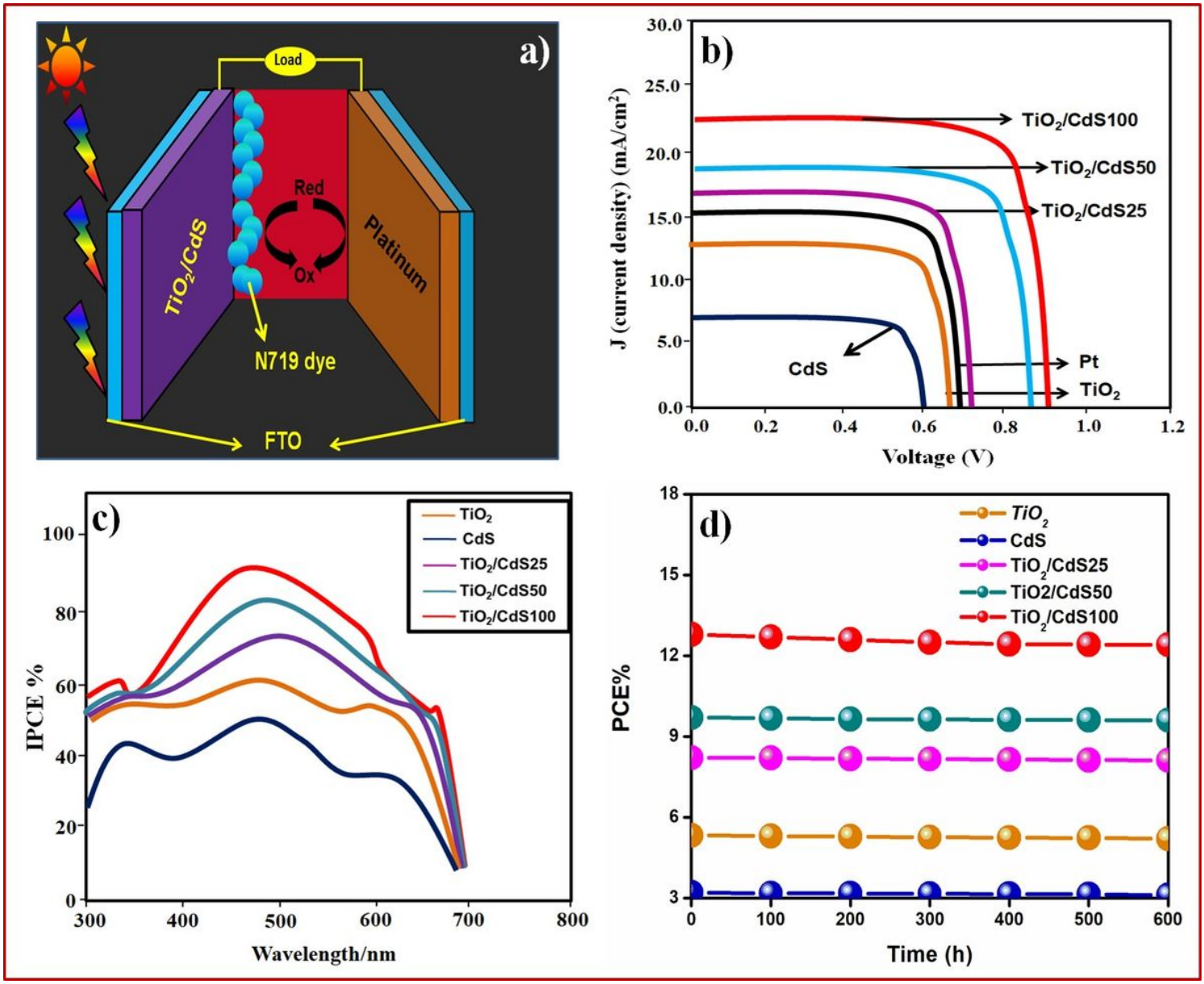

Figure 8

a) DSSC schematic sketch; b) J-V plot; c) IPCE spectra; d) stability test

Figure 9 Placeholder

Figure 9

(Figure 9 was not provided with this version of the Manuscript) a) EIS spectra with equivalent circuit (inset); b) photo conversion mechanism